

Mechanical Characterization of Pre-Fatigued Free-Cutting Steels under Dynamic Tension

Masaaki ITABASHI, Heikichi KOSEKI

Tokyo University of Science, Suwa
Department of Mechanical Systems Engineering
5000-1, Toyohira, Chino, Nagano 391-0292, Japan
itabashi@rs.suwa.tus.ac.jp

In the near future, toxic Pb will be prohibited to add to free-cutting steels. So far, many types of free-cutting steels without Pb have appeared. In order to compare dynamic mechanical properties of Pb added SUM24L steel (refer to JIS G 4804:2008, equivalent to AISI 12L14 steel) with those for Pb free SUM23 (equivalent to AISI 1215), high velocity tensile tests are carried out at a strain rate of $1 \times 10^3 \text{ s}^{-1}$, at room temperature. A half of the specimens are pre-fatigued before the dynamic tensile test. This loading combination, fatigue and impact, simulates a certain service condition, normal operational loadings and an accidental dynamic loading. Tensile strength of the pre-fatigued specimens is less than that of the virgin specimens, to some extent, for both steels. Where the degradation is of almost the same level, replacement of the Pb added free-cutting steel with the Pb free steel may be possible.

Key words: dynamic tension, pre-fatigue, Pb free, free-cutting steel, degradation.

1. INTRODUCTION

The loading combination of fatigue-impact is one of the more under-developed engineering fields. Some pioneer works exist and are as follows. MACGREGOR and GROSSMAN [1] found that for SAE1020 steel the ductile-brittle transition temperature of their cylindrical specimens with a circular notch tended to increase after rotary bending fatigue. NAKANISHI and HAZE [2] carried out Charpy impact tests for a normalized low carbon steel with pre-fatigue by pulsating tension. They also reported the increase of the transition temperature by pre-fatigue. With Vickers hardness test, SATO, IMAMURA and KAWARAI [3] tried to detect such an increase of the transition temperature with low-to-medium cycle pre-fatigue conditions for a rolled steel structure. Thus, these pioneering works focused on the variation of the ductile-brittle transition temperature.

From the structural designers' viewpoint, the remaining dynamic strength and toughness of the materials of interest are also needed for members and structure with good durability against fatigue-impact loading.

Recently, the loading axes of pre-fatigue and succeeding tensile impact coincided with each other in order to simulate the service condition of investigated materials more accurately with a high velocity tensile testing technique. For three Al alloys damaged by low-cycle pre-fatigue in sinusoidal pulsating tension, deterioration of dynamic tensile strength and elongation was reported by KAWATA, ITABASHI and KUSAKA [4]. AUZANNEAU [5] found that on the side surface of pre-fatigued and dynamically-tensile-fractured 2017-T3 Al alloy specimen, there existed opened cracks of large lengths, typically 400 μm . According to his experimental results, ITABASHI, NAKAJIMA and FUKUDA [6] observed the side surface of pre-fatigued and dynamically-fractured 6061-T6 and 2219-T87 Al alloys with a scanning electron microscope and found that the number of relatively large cracks was one of the indicators of the loading combination type with some screening techniques.

On the other hand, for steels, such a deterioration of mechanical properties was not found. ITABASHI and FUKUDA [7] found this fact for two steels for building structure. TSUDA, DAIMARUYA, KOBAYASHI and SUNAYAMA [8] also confirmed that even automotive sheet steels did not reveal such a deterioration with the fatigue-impact loading combination. They carried out to investigate that fact not only for low-cycle pre-fatigue, but also for high-cycle pre-fatigue. Therefore, these steels are stronger to the fatigue-impact loading in tension than the Al alloys.

For free-cutting steels, their mechanical properties are functionally degraded, especially the local toughness. The second phase exists in steel matrix, as a chip breaker, tool edge stabilizer, and tool life extender. For these purposes, the second phase plays the role of a solid lubricant. Typical materials as the second phase in free-cutting steels are Pb and MnS. The existence of the second phase can be recognized as the stress concentrated point in the steels. Under the fatigue-impact combination, a relatively larger deterioration of the mechanical properties of free-cutting steels should appear than that for general structural steels.

In this paper, to clarify the above-mentioned theme, two free-cutting steels, a Pb added steel and a Pb free one, are pre-fatigued by low-cycle pulsating tension and tested quasi-statically and dynamically in tension. It is needless to say that Pb is prohibited to be alloyed in steel by more than 0.35% mass, by the RoHS (restriction of hazardous substances) directive. In the near future, this allowable range will be disappeared. Comparing experimental results of the steels, the possibility of replacing the former steel with the latter can be argued from such a loading combination aspect.

2. EXPERIMENTAL PROCEDURE

2.1. Investigated free cutting steels

The Pb added free-cutting steel is SUM24L steel (JIS G 4804:2008, equivalent to AISI 12L14 steel). The capital letter “L” in the above symbols means lead. The Pb free steel is SUM23 steel (equivalent to AISI 1215 steel). The chemical composition of the steels are tabulated in Table 1. In JIS G 4804:2008, the mechanical properties of the free-cutting steels are not prescribed. The manufacturing process of both steels was the same and was as follows. Each steel was melted in a factory converter, cast continuously and rolled into a square bullet of 155×155 mm. The bullet was cut into an appropriate length, heated at 1250°C for 30 min, hot forged into a $\varnothing 12$ mm cylindrical bar and cooled in air. The hot-forging process was important to distribute grains of Pb and MnS uniformly and to adjust the grain size. This process is the same as commercially available SUM24L and SUM23 steels.

Table 1. Chemical composition for the free-cutting steels investigated here (unit: % mass).

Material	C	Mn	P	S	Cr	Pb	Fe
SUM24L	0.08	1.12	0.084	0.297	0.04	0.24	Bal.
SUM23	0.08	1.00	0.085	0.322	0.03	–	Bal.

The steels were supplied in $\varnothing 12$ mm cylindrical bars. The bars were machined to the specimen configuration as shown in Fig. 1. After turning, the parallel part with round fillets of the specimen was ground by #4000 emery paper.

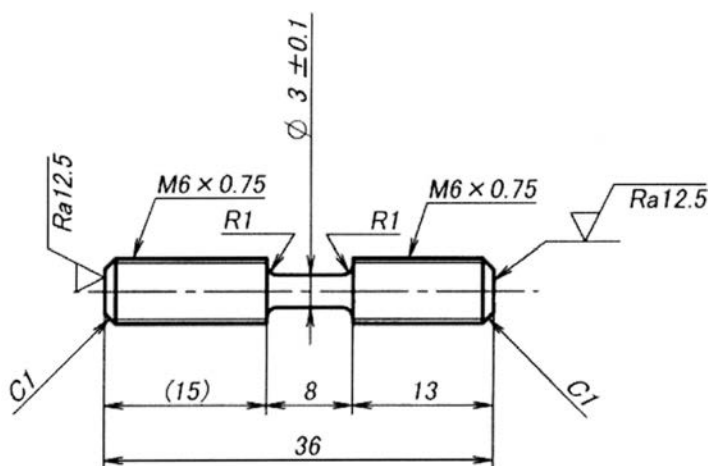


FIG. 1. Specimen configuration (in mm).

2.2. Quasi-static tensile test

At a strain rate of $1 \times 10^{-3} \text{ s}^{-1}$, quasi-static tensile tests were carried out with a servohydraulic fatigue testing machine (Shimadzu Corp., Servopulser EHF-FB1 type 1111, crosshead speed: 0.5 mm/min). To improve the accuracy of the elongation measurement, specially designed specimen attachments were introduced with two clip gauges (Tokyo Sokki Kenkyujo Co., Ltd., UB-5L, gauge length: 5 mm), as shown in Fig. 2.

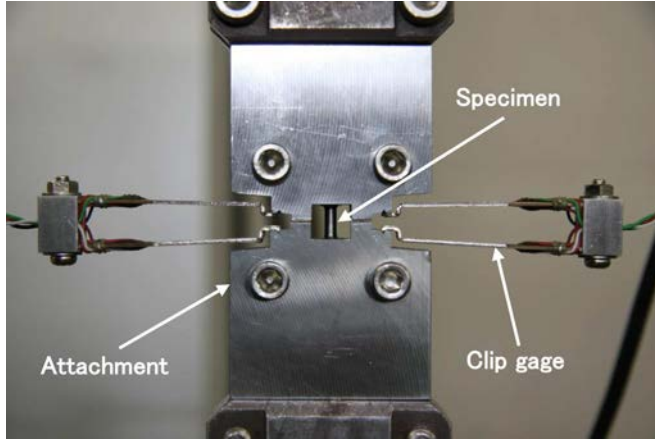


FIG. 2. Detail of the specially designed specimen attachments with two clip gauges for quasi-static tensile test.

At the beginning of this series of experiments, three quasi-static tensile tests for virgin (not pre-fatigued) specimens of each steel were executed. According to the quasi-static tensile strengths, fatigue test conditions were set appropriately.

2.3. Fatigue test and pre-fatigue conditions

For both steels, $S-N$ curves were obtained, respectively. The curves were evaluated under sinusoidal pulsating tension (stress ratio: 0, frequency: 20 Hz) by the servohydraulic fatigue testing machine. Circular plots in Fig. 3 are the results of the fatigue tests. Bold solid lines are linear fitted lines obtained by the least square method.

Complying with the conditions of Al alloys [4, 6], pre-fatigue conditions were decided as follows. Maximum (pre-fatigue) stresses were set at 78 and 89% of the quasi-static lower yield strength, as shown in Fig. 3, i.e., 343 and 392 MPa for SUM24L steel, and 319 and 364 MPa for SUM23. Square and rhombic plots indicate (pre-fatigue) cycle ratios, 5 and 20% of the number of cycles to failure respectively. These severe conditions were the onset of the tensile strength degradation for the formerly investigated Al alloys [4, 6].

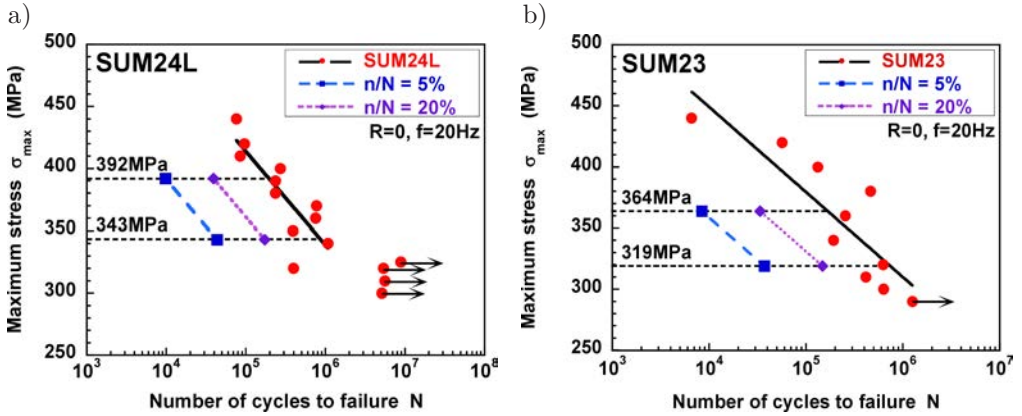


FIG. 3. S - N curves and pre-fatigue conditions: a) SUM24L steel, b) SUM23 steel.

2.4. Preparation of pre-fatigued specimens

With the servohydraulic fatigue testing machine, five pre-fatigued specimens were prepared for each pre-fatigue condition. Several specimens for SUM24L steel were fractured during the pre-fatigue. For SUM23 steel, no specimen was fractured during preparation.

2.5. Dynamic tensile test

Tensile tests at a dynamic strain rate of approximately $1 \times 10^3 \text{ s}^{-1}$, were carried out with a high velocity tensile testing machine of a horizontal slingshot type [9]. This machine adopted the one bar method [10] to obtain dynamic stress-strain curves without ringing.

The principle of the one bar method is shown in Fig. 4. It consists of three elements, an impact block as a rigid body, a specimen, and an output bar as an elastic bar. Deriving from the one-dimensional elastic wave propagation theory and Hooke's law, the fundamental formulae for dynamic stress $\sigma(t)$, dynamic strain $\varepsilon(t)$ and strain rate $\dot{\varepsilon}(t)$ in nominal are as follows:

$$(2.1) \quad \sigma(t) = \frac{S_0}{S} E_0 \varepsilon_g \left(t + \frac{a}{c} \right),$$

$$(2.2) \quad \varepsilon(t) = \frac{1}{\ell} \int_0^t \left\{ V(\tau) - c \varepsilon_g \left(\tau + \frac{a}{c} \right) \right\} d\tau,$$

$$(2.3) \quad \dot{\varepsilon}(t) = \frac{1}{\ell} \left\{ V(t) - c \varepsilon_g \left(t + \frac{a}{c} \right) \right\},$$

where t is the time after impact, ℓ and S are the gauge length and cross-sectional area of the specimen, S_0 , E_0 and c are the cross-sectional area, Young's modulus,

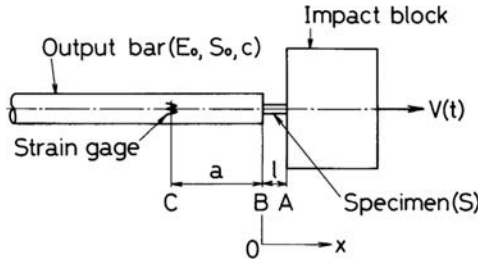


FIG. 4. Principle of the one bar method.

and longitudinal elastic wave velocity of the output bar, $V(t)$ is the velocity of the impact block, and $\epsilon_g(t)$ is the strain of the output bar at the distance a from the loaded end.

The tensile impact load was generated by the horizontal slingshot machine. A hammer made of carbon steel, 50 kg in mass, can be accelerated to the velocity of 5–6 m/s. The accelerated hammer impinged on the impact block made of chromium molybdenum steel. The impact block of 0.7 kg in mass and $20(H) \times 60(L) \times 75(W)$ mm³ in size, flew at the higher velocity, typically 7–8 m/s, than that of the hammer. Therefore, the maximum nominal strain rate attained 0.7×10^3 – 0.8×10^3 s⁻¹ with the specimen of an initial gauge length of 8 mm.

Figure 5 shows a block diagram of the dynamic data acquisition system. In order to detect $\epsilon_g(t)$, four semiconductor strain gauges (Kyowa Electronic Instruments, KSP-2-120-E3, gauge length: 2 mm, gauge factor: 120) were cemented onto the output bar made of type 304 stainless steel, at the location of 50 mm (= a) apart from the specimen-mounted end. The output bar was 3 m in length and $\phi 10$ mm in diameter. The displacement of the impact block,

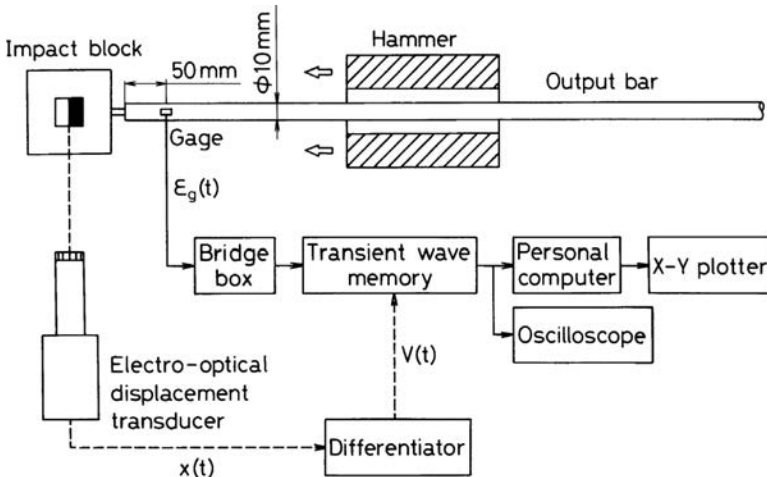


FIG. 5. Block diagram of dynamic data acquisition system for tensile stress-strain relation.

$x(t)$ was detected by an electro-optical displacement transducer (Zimmer Model 100D/II, gauge length of an installed lens: 10 mm). This signal was differentiated with respect to time by a differentiator (Zimmer Model 131C) in order to obtain the velocity of the block, $V(t)$. The output bar strain $\varepsilon_g(t)$ and impact block velocity $V(t)$ were stored in two synchronized digital memories (Kawasaki Electronica, TMR-100, sampling frequency: 1 MHz, resolution: 10 bits, memory length: 4 kwords).

3. RESULTS AND DISCUSSION

3.1. Obtained stress-strain curves

The tensile stress-strain curves for the virgin specimens up to fracture are shown in Fig. 6 and for the pre-fatigued specimens in Fig. 7. The stress-strain

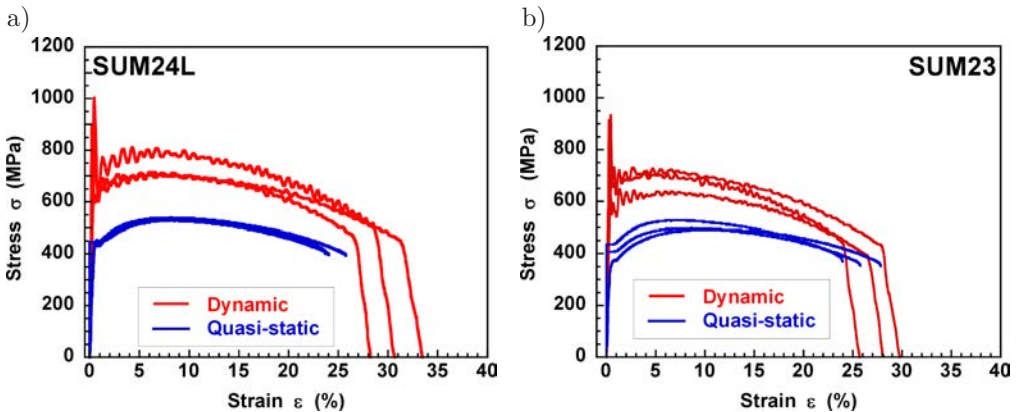


FIG. 6. Tensile stress-strain curves for virgin specimens: a) SUM24L steel, b) SUM23 steel.

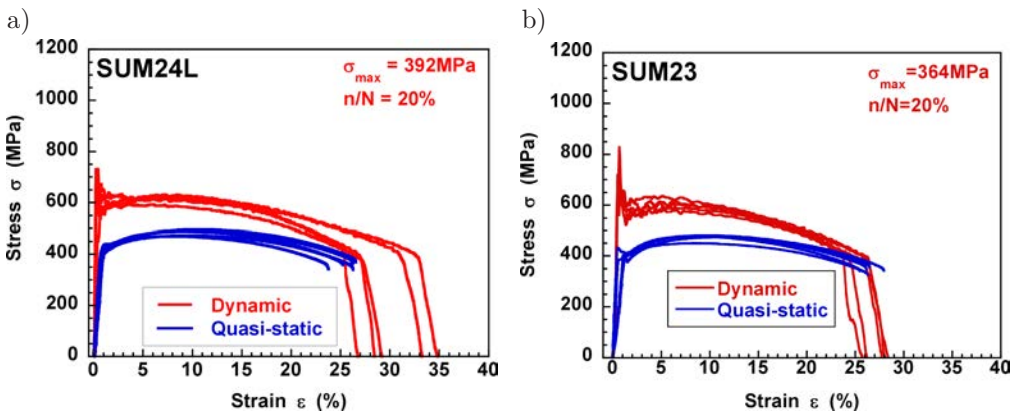


FIG. 7. Tensile stress-strain curves for pre-fatigued specimens ($\sigma_{\max} = 392$ MPa for SUM24L steel and 364 MPa for SUM23 steel, $n/N = 20\%$): a) SUM24L steel, b) SUM23 steel.

curves for both steels shown in Fig. 6 are standards of a succeeding series of the present experiments. Generally speaking, the virgin curves are higher than the pre-fatigued curves. The pre-fatigue condition in Fig. 7 is the severest one for each steel; thus there is an obvious deterioration of flow stress, but it is not so much, typically 100–150 MPa.

3.2. Remaining strength

The fatigue cycle ratio dependence of the deterioration of the remaining (tensile) strength is shown in Figs. 8 and 9. Taking fatigue cycle ratio as an abscissa, the results of the virgin specimen correspond to plots of $n/N = 0\%$. The number of plots of $n/N = 0$ is three, and those of $n/N = 5\%$ and 20% are

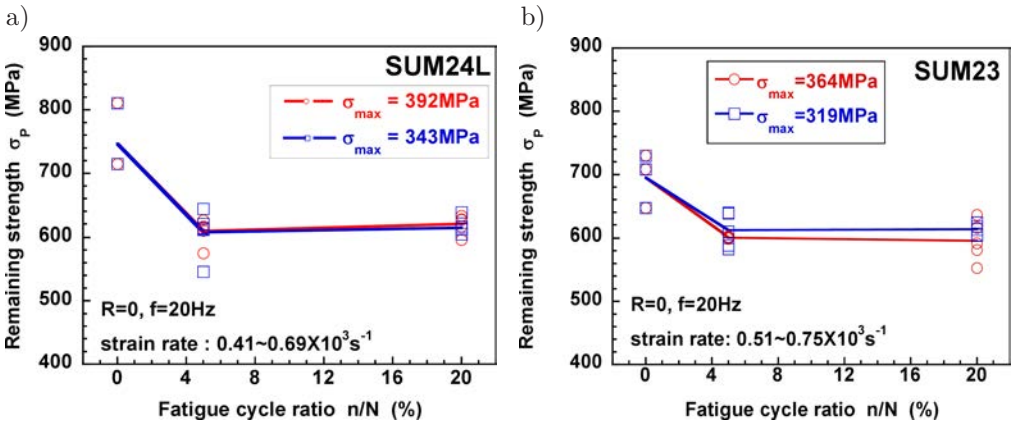


FIG. 8. Fatigue cycle ratio dependence of dynamic tensile strength for free-cutting steels: a) SUM24L steel, b) SUM23 steel.

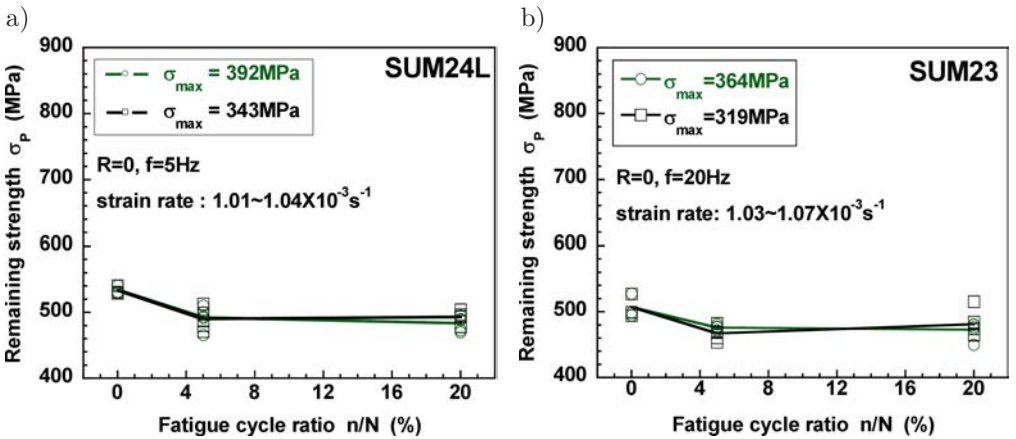


FIG. 9. Fatigue cycle ratio dependence of quasi-static tensile strength for free-cutting steels: a) SUM24L steel, b) SUM23 steel.

five for each maximum (pre-fatigue) stress. In Fig. 8, even with the virgin condition, plots are widely scattered. The cause of this scatter may be the relatively small specimen diameter, since grains of the second phase were not so uniformly distributed in the gauge length of the specimen. Beyond the scattering width, the remaining dynamic strength in Fig. 8 deteriorates at a ratio of 5% for both steels. But, this lowered strength is maintained at 20%. From the viewpoint of well-known damage mechanics, this tendency is unusual. In such a case, the remaining strength will decrease monotonously with increasing cycle ratio. On the contrary, for these free-cutting steels, it does not seem unusual that the steel matrix around the second phase can be hardened by stress concentration. Therefore, between the ratio of 5% and 20%, it is possible to explain that some weakening of the total strength by pre-fatigue is balanced with some hardening of the local stress concentration. In Fig. 9, the deterioration of quasi-static remaining strength is smaller than that of dynamic one. The quasi-static strength for both steels keeps the constant level between the fatigue cycle ratio of 5% and 20% too.

The deterioration of the remaining strengths at both strain rates does not depend on maximum (pre-fatigue) stresses. This suggests that the second phase, Pb and MnS have been debonded from the matrix due to the weak strength of the second phase itself during pre-fatigue. This hypothesis can be confirmed by lowering the maximum (pre-fatigue) stress level to the tensile strength of Pb, typically 10 MPa. Then, such deterioration at the fatigue cycle ratio of 5% will be reduced.

3.3. Breaking strain

The breaking strain in a dynamic tensile test tends to scatter. The distributed second phase in free-cutting steels is one of the main factors of fracture. Dynamic breaking strain of the free-cutting steels is widely scattered, as shown in Fig. 10. In general, the pre-fatigue decreases the breaking strain, except for the condition of $\sigma_{\max} = 364$ MPa and $n/N = 5\%$. It can be thought that Pb and MnS were not so uniformly distributed even after the hot-forging process. On the other hand, quasi-static breaking strain gives the opposite tendency, as shown in Fig. 11. In the second phase, Pb and MnS may be the cause of these different tendencies. At the quasi-static strain rate, the soft second phase helps necking growth, easily deforming from the original shape in the hard matrix.

This scattering of these breaking strains may be reduced by utilizing larger specimens, for example, $\varnothing 10$ mm in diameter. This value is comparable to a standardized quasi-static tensile specimen. According to the capacity of dynamic tensile testing machine, the diameter of the parallel part of the present specimen is only $\varnothing 3$ mm.

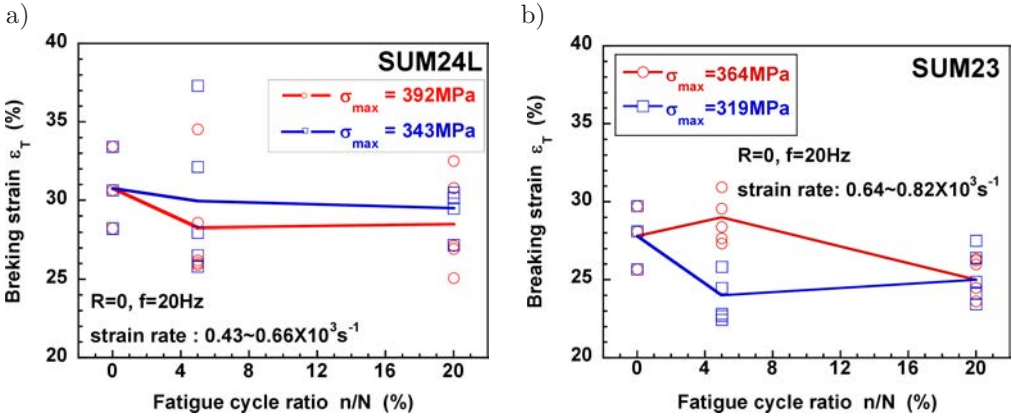


FIG. 10. Fatigue cycle ratio dependence of dynamic breaking strain for free-cutting steels: a) SUM24L steel, b) SUM23 steel.

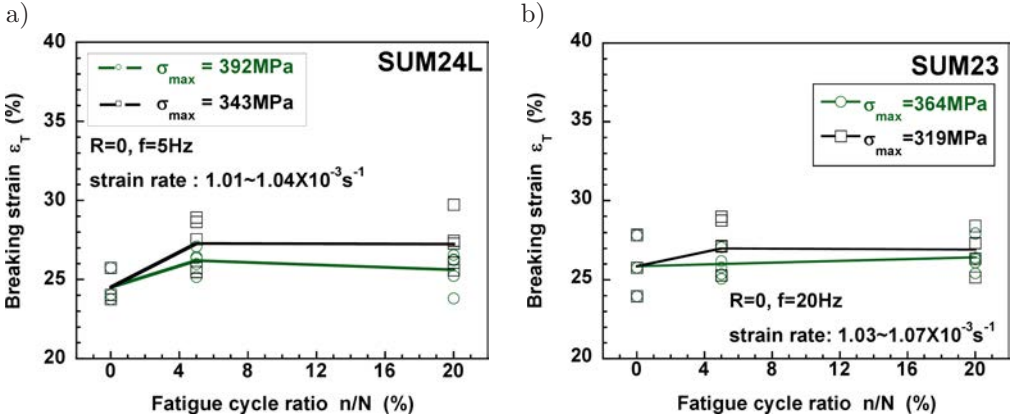


FIG. 11. Fatigue cycle ratio dependence of quasi-static breaking strain for free-cutting steels: a) SUM24L steel, b) SUM23 steel.

3.4. Absorbed energy per unit volume

The dynamic absorbed energy per unit volume is an important factor of impact resistance. Figure 12 shows the deterioration of dynamic absorbed energy. For SUM23 steel at $n/N = 5\%$, the dynamic absorbed energy of $\sigma_{\max} = 364\text{MPa}$ is larger than 319MPa . No rational explanation can be given for this tendency; however, this tendency reflects the dynamic breaking strain tendency of Fig. 10b. Quasi-static absorbed energy is relatively stable, as shown in Fig. 13. The deterioration of strength is recovered by the slight increase of breaking strain.

From the obtained results, the pre-fatigue affects the impact tensile resistance of the free-cutting steels intensely. However, the dynamic strengths and absorbed energies are always higher than the quasi-static ones. Thus, the strain rate effect on the absorbed energy per unit volume is superior to the pre-fatigue effect.

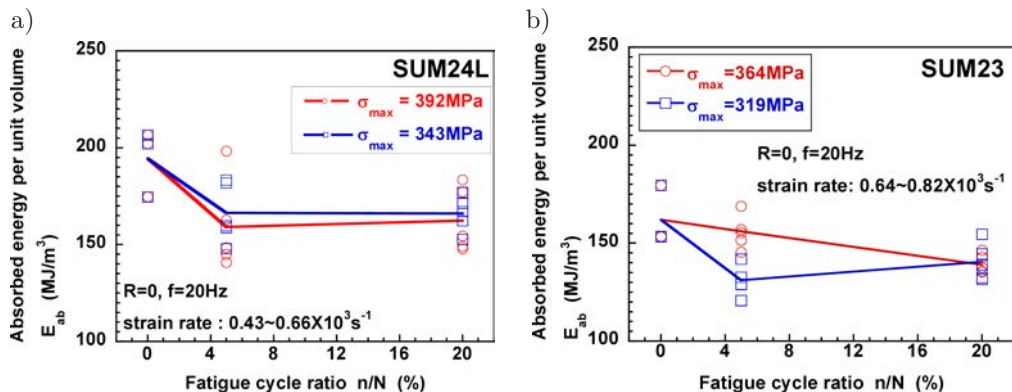


FIG. 12. Fatigue cycle ratio dependence of dynamic absorbed energy per unit volume for free-cutting steels: a) SUM24L steel, b) SUM23 steel.

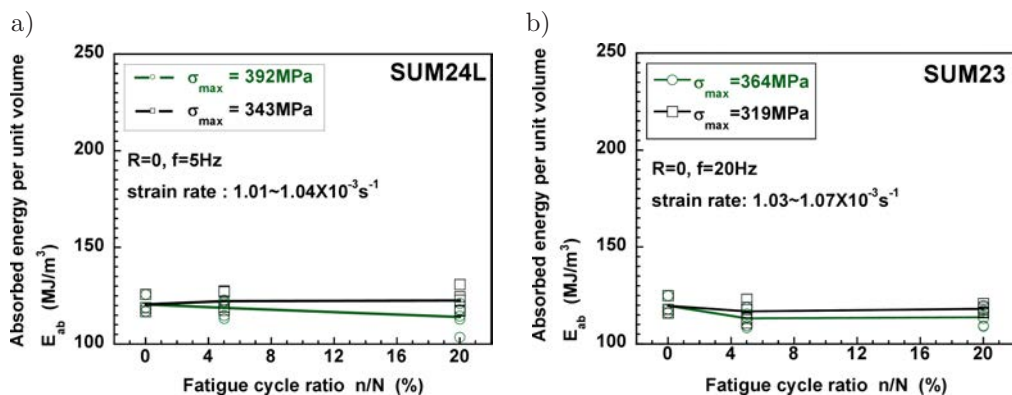


FIG. 13. Fatigue cycle ratio dependence of quasi-static absorbed energy per unit volume for free-cutting steels: a) SUM24L steel, b) SUM23 steel.

4. CONCLUSIONS

A Pb added free-cutting steel, SUM24L (equivalent to AISI 12L14) steel, and a Pb free free-cutting steel, SUM23 (AISI 1215) steel, were investigated to confirm the tensile impact resistance with the severe pre-fatigue conditions. Generally speaking, the pre-fatigue has a negative effect on the strength of free-cutting steels, at not only the quasi-static strain rate of $1 \times 10^{-3} \text{s}^{-1}$, but also the dynamic strain rate of $1 \times 10^3 \text{s}^{-1}$. Regardless of the strain rate, the pre-fatigue process makes the scatter of mechanical properties wider. The weakened bonding and debonding between the matrix and second phase may be one of the main causes of the scatter and deteriorated mechanical properties. From the dynamic tensile stress-strain curves for both steels, 20%-reductions in strength and absorbed energy are observed respectively. From the quasi-static curves, 10%-reductions in strength and absorbed energy are obtained. Both steels reveal that they have almost the same mechanical properties and the same tendencies

to the present fatigue-impact loading combination. Thus, SUM24L steel can be replaced with SUM23 in this particular simulation.

This article discusses only phenomenological aspects. However, such degradation of these mechanical properties for the investigated free-cutting steels has not been published as far as the authors know. In the near future, the mechanical damage of the interface between the steel matrix and second phase will be observed microscopically, and the affect of the interface on the observed pre-fatigue effect will be investigated and reported.

REFERENCES

1. MACGREGOR C.W., GROSSMAN N., *Some New Aspects of the Fatigue of Metals Brought out by Brittle Transition Temperature Tests*, The Welding Journal, Welding Research Supplement, **27**, 132-s-143-s, 1948.
2. NAKANISHI S., HAZE T., *The Change of Impact Characteristics under the Repeating Load* [in Japanese], Tetsu-to-Hagane, **52**, 4, 654–656, 1966.
3. SATO S., IMAMURA Y., KAWARAI, T., *Determination of Increase in Brittle Transition Temperature of Steel Due to Fatigue by Hardness Test* [in Japanese], Journal of the Society of Materials Science, **25**, 270, 290–295, 1976.
4. KAWATA K., ITABASHI M., KUSAKA S., *Behaviour Analysis of Pre-Fatigue Damaged Aluminum Alloys under High-Velocity and Quasi-Static Tension*, [in:] IUTAM Symposium on Micromechanics of Plasticity and Damage of Multiphase Materials, Pineau A., Zaoui A. [Eds.], Kluwer Academic Publishers, Dordrecht, 397–404, 1996.
5. AUZANNEAU T., *Influence d'un Pré-Endommagement par Fatigue sur la Tenue au Choc – Application à un Alliage d'Aluminium 2017A T3* [in French], PhD Thesis, Ecole Nationale Supérieure d'Arts et Métiers, Bordeaux, France, 1999.
6. ITABASHI M., NAKAJIMA S., FUKUDA, H., *Microscopic Observation of the Side Surface of Dynamically-Tensile-Fractured 6061-T6 and 2219-T87 Aluminum Alloys with Pre-Fatigue*, JSME International Journal, Ser. A, **48**, 4, 222–227, 2005.
7. ITABASHI M., FUKUDA H., *High Velocity Tensile Mechanical Behavior for Low-Cycle Pre-Fatigued SN490B Steel (Rolled Steel for Building Structure)* [in Japanese], Journal of the Society of Materials Science, Japan, **53**, 3, 260–265, 2004.
8. TSUDA H., DAIMARUYA M., KOBAYASHI H., SUNAYAMA Y., *Effect of Pre-Fatigue on Impact Tensile Properties of Laser Welded Butt Joint of High Strength Steel Plates* [in Japanese], Journal of the Society of Materials Science, Japan, **55**, 9, 824–830, 2006.
9. ITABASHI M., KAWATA K., *Carbon Content Effect on High-Strain-Rate Tensile Properties for Carbon Steels*, International Journal of Impact Engineering, **24**, 2, 117–131, 2000.
10. KAWATA K., HASHIMOTO S., KUROKAWA K., KANAYAMA N., *A New Testing Method for the Characterization of Materials in High Velocity Tension*, [in:] *Mechanical Properties at High Rates of Strain 1979*, Institute of Physics Conference Series No. 47, Harding J. [Ed.], Institute of Physics, Bristol and London, 71–80, 1979.

Received December 20, 2010; revised version January 31, 2013.
